



ELSEVIER

Chemical Engineering Science III (III) III-III

Chemical
 Engineering Science

www.elsevier.com/locate/ces

Viscous fluid mixing in a tilted tank by periodic shear

Thomas Ward^{a,*}, Asher Metchik^b

^aDepartment of Mathematics, University of California, Los Angeles, CA 90095-1555, USA

^bDepartment of Mechanical and Aerospace Engineering, University of California, Los Angeles, CA 90095-1597, USA

Received 1 April 2007; received in revised form 4 July 2007; accepted 17 July 2007

Abstract

A tilted-partially filled rotating tank is studied, both experimentally and theoretically at small Reynolds and capillary numbers, to study mixing viscous fluid by periodic shear. The maximum mixed cross-sectional area, $A_{\max}(\alpha) = A(\Delta t_{\max}(\alpha))$, and mixing rate, $1/\Delta t_{\max}(\alpha)$, are estimated as a function of the flow parameters, which are the tilt angle, α , and free surface height, H_0 . A nonlinear flow model is found by expanding linear solid body rotation about a curved rotation axis that is needed to satisfy the zero shear stress and no normal velocity component for the flow in the vicinity of the free surface. A linear analysis of the nonlinear solution reveals an underlying periodic shear that is responsible for fluid mixing. The analysis suggests that the rate of mixing per unit area is a maximum near $\alpha = 52\pi/180$. Laser fluorescence experiments are performed to examine the mixing patterns via experimental Poincaré mapping [Fountain, G.O., Khakhar, D.V., Ottino, J.M., 1998. Visualization of three-dimensional chaos. *Science* 281, 683–686.]. Steady-state images of the mixed cross-sectional area are compared with the theory as a function of the flow parameters.

© 2007 Published by Elsevier Ltd.

Keywords: Fluid mixing; Periodic shear; Chaotic advection; Low-Reynolds-number flow

1. Introduction

Batch mixing of viscous fluids is of importance to industries such as food and chemical processing and has been a topic of academic interest for many years. The interest is in determining the most efficient way to mix fluids, so the practical problem involves both time and money, as well as a way to quantify mixing. In industry, it is common to achieve fluid mixing by generating turbulence in large cylindrical tanks. Turbulence is often generated by rapidly rotating fluid inside the tank with an array of impellers or disks, and also varying the internal geometry with baffles (Aubin and Xuereb, 2006; Campolo et al., 2003). This practice can result in large power requirements because it takes large Reynolds numbers to achieve even laminar mixing of viscous fluid in large cylindrical geometries. Even at high rotation rates there is no guarantee that mixing is achieved because Kolmogorov–Arnold–Moser, or KAM (Arnold, 1978), surfaces typically develop (Alvarez-Hernández et al., 2002).

The only mixing from KAM regions is by diffusion which is the rate limiting step in any mixing process. Recently, researchers have proposed using chaotic advection to break up these KAM surfaces by transporting fluid to these regions to generate good mixing (Aref, 1984). Instead we propose an alternative to batch mixing of viscous fluids by periodic shearing (Franjone and Ottino, 1992; D’Alessandro et al., 1999) in a tilted-slowly rotating tank. This process of mixing fluids is analogous to a cement mixer so it only requires one moving part and the power requirements to rotate a tank are independent of the fluid viscosity. In this paper we provide an estimate of the mixed cross-sectional area and mixing rate for a steady flow generated by a tilted-slowly rotating tank generated by periodic shearing.

Alvarez-Hernández et al. (2002) performed a very detailed experimental and numerical investigation of the shortcomings of rapidly rotated batch-type mixers. The authors compare a variety of impeller and disk arrangements in cylindrical tanks and examine the mixing behavior under laminar flow conditions. Surprisingly, they found that a large portion of the power used to stir the fluid does not actually aid in mixing because of KAM-type surfaces that are always preserved. To achieve better

* Corresponding author. Fax: +1 310 206 6673.
 E-mail address: tward@math.ucla.edu (T. Ward).

1 mixing, the authors suggest using closely offset impeller to
 2 break up these regions, which increased the percent coverage
 3 of the mixed area from a maximum of about 20%, for regu-
 4 lar Rushton-type impellers, to approximately 25% for the off-
 5 set impellers. Fountain et al. (2000) also studied the problem
 6 of fluid mixing in a tank, but with a tilted disk and at $O(1)$
 7 Reynolds numbers. In their paper, they present some exper-
 8 imental and theoretical analysis of KAM surfaces generated
 9 by chaotic advection. To break up the KAM surfaces the au-
 10 thors design a tank that also rotates about a fixed axis, which
 11 achieved very good mixing in a much shorter time than with-
 12 out the secondary motion. While, so far, most of the studies
 13 have provided insight into the dynamics of mixing processes
 14 (i.e. KAM surfaces), they do not provide an estimate of the
 15 mixed domain size, mainly because the comprehensive analysis
 16 of Lagrangian particle trajectories requires large-scale three-
 17 dimensional computation at small or large Reynolds numbers
 18 in cylindrical geometries.

19 Consider a fluid in a partially filled tank of radius R , and fluid
 20 height H_0 rotating about an axis \mathbf{e}_{z_α} with respect to the horizon
 21 in the limit of low Reynolds and capillary number. For $\mathbf{e}_z \neq \mathbf{e}_{z_\alpha}$
 22 the free surface normal and the tank solid body axis of rotation
 23 are not parallel (see Fig. 1). So the liquid rotation axis is not
 24 equal to the solid body rotation axis because it must be curved
 25 in order to satisfy the zero stress and zero normal velocity,
 26 along with continuity at the free surface H_0 . We will develop
 27 an approximate model for the tilted rotating tank by expanding
 28 linear solid body rotation about a curved liquid axis of rotation
 29 that satisfies these three conditions, but not the no slip condition
 30 at the wall. If the mixing is due to periodic shear then there is
 31 no need to satisfy no slip at the wall since the mixing is due to
 32 flow around the liquid rotation axis. Trajectories in the vicinity
 33 of the free surface will depend on \tilde{z} , where \tilde{z} denotes variables

used to represent location along the liquid rotation axis. From
 here on all lengths are scaled by R , time by Ω , and area by
 R^2 . With this choice of scaling for the time, the time elapsed
 is equal to the number of rotations.

In dimensionless terms the free surface is located at $z =$
 $1/\lambda$ with $\lambda = R/H_0$. The applicable domain for the model is
 confined to a region spanning the free surface, $\Delta x = 2 \sec \alpha$
 (see Fig. 1), which is the distance bounded by the left and
 right liquid–vapor–solid triple points. The disturbed velocity
 field does not exist for all z because the orientations of the
 streamline and rotation axis are perpendicular at \tilde{z}_{crit} . This is
 adjacent (right side) to the region spanning the free surface
 Δx . So the vertical distance between the free surface and a
 trajectory located at $z = \tilde{z}_{\text{crit}}$, denoted $1/\lambda_{\text{crit}}(\alpha)$, can provide us
 with an estimate of the maximum area of the mixed domain,
 denoted by $A_{\text{max}}(\alpha)$, assuming all of the flow in this domain is
 being disturbed. We find the expression $1/\lambda_{\text{crit}}(\alpha) = 2 \sin \alpha$ by
 using the tank diameter and geometry. Now we propose that
 the maximum dimensionless mixed cross-sectional area as the
 triangular area in Fig. 1(a) or

$$A_{\text{max}}(\alpha) = 2 \tan \alpha. \quad (1)$$

This analysis suggests that the mixed domain sizes are similar
 so that they are independent of the liquid level for $\lambda \geq \lambda_{\text{crit}}$.
 If this expression is correct then it also would suggest that
 mixing is generated by disturbing the flow in the vicinity of
 the free surface, as we have proposed. We see that a non-tilted
 tank produces a vertical mixed domain size of exactly zero,
 while the fully tilted tank, $\alpha = \pi/2$, has a mixed domain size
 that diverges. But the flow for $\alpha = \pi/2$ is two-dimensional and
 cannot transport fluid along the axis of rotation even though
 the mixed area diverges (Unger et al., 2000).

In the vicinity of the liquid rotation axis we have $\mathbf{v}(\tilde{\mathbf{x}}) \approx 0$
 so that one can describe fluid trajectories using the phase angle
 relationship

$$\theta(\tilde{z}) = \omega(\tilde{z})t. \quad (2)$$

The frequencies, $\omega(\tilde{z})$, are eigenvalues of the associated non-
 linear advection equation about the liquid rotation axis. This
 analysis implies that the eigenvalue expansion about the rota-
 tion axis reveals a flow similar to solid body rotation, with a
 velocity gradient tangent to the liquid rotation axis.

Fluid transport tangent to the rotation axis is not possible
 with the linear equation, since particles travel along closed
 curves. So fluid mixing, if it occurs, is done by stretching of
 material lines by periodic shearing (Franjione and Ottino, 1992;
 D'Alessandro et al., 1999). Stretching occurs when material
 lines (a set of trajectories) sample an initial trajectory plane,
 defined as $\Delta\theta(\tilde{z}) = \theta(\tilde{z}_{\text{crit}}) - \theta(1/\lambda) = 0$ at time $t = 0$, at dif-
 ferent rates. Since the flow is steady and periodic the trajec-
 tories diverge from $\Delta\theta(\tilde{z}) = 0$ as $t \rightarrow \infty$, but they must sam-
 ple the initial plane periodically when $t = 2\pi/\Delta\omega(\tilde{z})$, where
 $\Delta\omega(\tilde{z}) = \omega(\tilde{z}_{\text{crit}}) - \omega(1/\lambda) = 1 - \omega(1/\lambda)$. So material lines
 that are initial along a line will fill a plane as $t \rightarrow \infty$. But, in
 practice, this kinematic description for the flow fails when the
 distance between trajectories is less than the diffusion length,

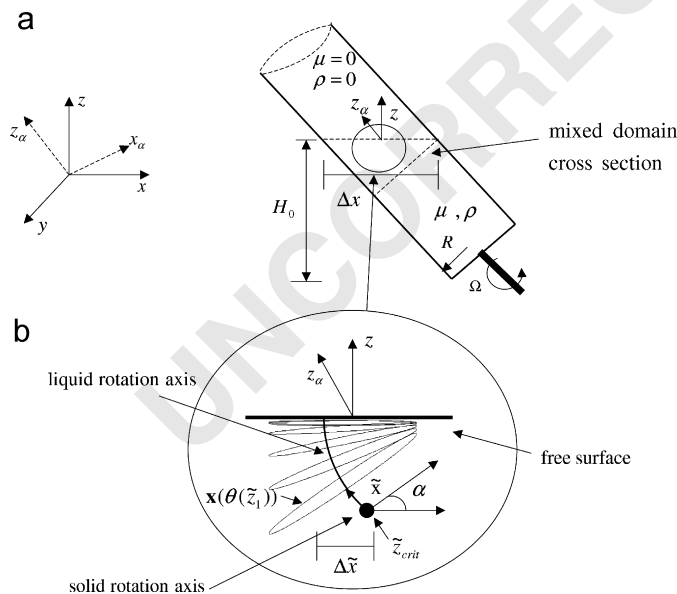


Fig. 1. (a) Problem schematic. (b) Close-up illustration of fixed point axis orientation relative to the other axis. (c) Trajectories at different locations along fixed point axis. The trajectories are all similar but have different orientations so that particles do not travel at the same velocity.

and this is how mixing is achieved. This process is analogous to the discontinuous flow models used by Franjone and Ottino (1992) for an eggbeater-type flow and by D'Alessandro et al. (1999) for periodic shearing in two directions. In our problem the periodic boundary conditions are replaced by a liquid rotation axis.

In practical terms, if the phase angle relationship holds then the rate of deformation is independent of time or, $\Delta\dot{\theta} \propto \Delta\omega(\tilde{z})$, where the over-dot denotes a derivative with respect to time. We propose then that the deformation rate per unit cross-sectional area is proportional to the rate of mixing:

$$\frac{\Delta\dot{\theta}}{A_{\max}(\alpha)} \propto \frac{1}{\Delta t_{\max}(\alpha)}, \quad (3)$$

where $\Delta t_{\max}(\alpha)$ is the total elapsed time to completely mix area $A_{\max}(\alpha) = A(\Delta t_{\max}(\alpha)) = 2 \tan \alpha$ and $\Delta\dot{\theta} = 1 - \omega(1/\lambda)$. If this expression is the rate determining step then it will give us an estimate for the rate of mixing, $1/\Delta t_{\max}(\alpha)$, that can be compared with experimental measurements. Such a flow would have a zero Lyapunov exponent because the mixing is due to linear stretching, i.e. $\Delta\theta \propto t$, and not exponential separation of trajectories. An expression for the function $\omega(1/\lambda)$ is found in the following sections.

In the next section the theory describing the analytical technique to determine the size of the mixed domain is presented. The solution is analyzed and compared with experiments that are presented in Section 3. The experiments and theory for the size of the mixed area and the mixing time $\Delta t_{\max}(\alpha)$ are compared in the following section and conclusions are presented at the end.

2. Analysis and results

An approximate nonlinear advection equation for the steady flow generated in a tilted rotating tank is found by expanding linear solid body rotation about the fixed point axis, $\mathbf{v}(\tilde{\mathbf{x}}) = 0$. The additional boundary conditions that will be satisfied are zero shear stress and zero normal velocity along the free surface at $z = 1/\lambda$, with $\lambda = R/H_0$. With this approximation we cannot satisfy the no slip conditions at the wall which leads to a secondary flow. But since we have proposed that mixing is due to periodic shearing we will only need an approximate form for the fixed points to determine $\omega(1/\lambda)$.

2.1. Tilted rotating tank model

Consider a Newtonian fluid, with viscosity μ , and density ρ , rotating slowly in a tank. The tank rotates about the z_α -axis and is tilted with an angle, α , about the y -axis (see Fig. 1). The free surface located at $z = 1/\lambda$ remains flat provided the capillary number $Ca = \mu\Omega R/\gamma$, where γ is the surface tension, is less than unity. So, for a partially filled tank in the limit of negligible convective momentum transport, or equivalently small Reynolds number, $Re = \rho\Omega R^2/\mu \ll 1$, the slow rotation causes a disturbance to the flow in the vicinity of the free surface. The dimensionless Stokes flow equations governing

momentum transport and continuity for the rotating-tilted tank are $\nabla \cdot \boldsymbol{\sigma} = 0$ where $\boldsymbol{\sigma} = -P\mathbf{I} + \boldsymbol{\tau}$ and $\nabla \cdot \mathbf{v} = 0$, respectively. The equations are made dimensionless using the characteristic length, R , and velocity scale, ΩR .

A general form of the perturbed autonomous advection equation $\dot{\mathbf{x}} = \mathbf{v}(\mathbf{x})$ governing solid body rotation in a tilted geometry is

$$\begin{pmatrix} \dot{x} \\ \dot{y} \\ \dot{z} \end{pmatrix} = \begin{pmatrix} y \cos \alpha \\ 1 - x \cos \alpha - z \sin \alpha + (f(y) + g(z)) \sin \alpha \\ y \sin \alpha + h(y, z) \sin \alpha \end{pmatrix}, \quad (4)$$

where the function f , g , and h are to be determined by satisfying continuity in the bulk and zero stress and normal velocity conditions along the free surface.

The normal stress components must satisfy $\mathbf{e}_z \cdot \boldsymbol{\tau} \cdot \mathbf{e}_x = 0$ and $\mathbf{e}_z \cdot \boldsymbol{\tau} \cdot \mathbf{e}_y = 0$ along the free surface at $z = 1/\lambda$. The normal velocity component vanishes along the free surface, or $\mathbf{e}_z \cdot \mathbf{v} = 0$, and we must also satisfy continuity. A power series for each unknown term is used to find the functions i.e. $f(y) = C_1 y^p$, $g(z) = C_2 z^q$, and $h(y, z) = C_3 y z^r$. The function $h(y, z)$ must be linear in y to satisfy the zero normal velocity boundary condition along the free surface. After applying the boundary conditions, $(\partial/\partial z)u(y) = 0$, $(\partial/\partial z)v(x, y, z = 1/\lambda) = 0$, $w(y, z = 1/\lambda) = 0$, and continuity, the particle trajectories near the fixed point axis for the rotating-partially filled-tilted tank are

$$\begin{pmatrix} \dot{x} \\ \dot{y} \\ \dot{z} \end{pmatrix} = \begin{pmatrix} y \cos \alpha \\ 1 - x \cos \alpha - z \sin \alpha + \frac{\lambda}{2}(z^2 + y^2) \sin \alpha \\ y \sin \alpha (1 - \lambda z) \end{pmatrix}. \quad (5)$$

The system of equations represents the approximate solution for the flow in the rotating tank. As $\alpha \rightarrow 0$ the solution is exact for the fluid problem of two-dimensional solid body rotation. But for large $\lambda \sin \alpha$ the solutions to this nonlinear differential equation are three-dimensional closed curves, and are neither volume filling nor a very good model for the fully three-dimensional flow. But the nonlinear model possesses a fixed point axis in the xz -plane of the form $x = ((\lambda/2)z^2 - z) \tan \alpha + \sec \alpha$. So while our nonlinear model is not a good global fluid model, it is exact near the fluid rotation axis since we can Taylor expand any function in the vicinity of a fixed point.

The fixed point axis lies in the xz -plane, $\tilde{\mathbf{x}} = (\tilde{x}(\tilde{z}), 0, \tilde{z})$ where

$$\tilde{x}(\tilde{z}, \alpha) = \left(\frac{\lambda}{2} \tilde{z}^2 - \tilde{z} \right) \tan \alpha + \sec \alpha. \quad (6)$$

This quadratic equation, of constant curvature $d^2 \tilde{x}/d\tilde{z}^2 = \lambda \tan \alpha$, is a parabola representing a family of fixed points emanating from the free surface at $1/\lambda$ to the rotating tank axis away from the interface. The tangent line to the fixed point axis is

$$\tilde{m}(\tilde{z}) = (\lambda \tilde{z} - 1) \tan \alpha \quad (7)$$

and the normalized vector tangent to the fixed point axis is

$$\tilde{\mathbf{m}} = (m_x, m_y, m_z) = \frac{1}{\sqrt{1 + \tilde{m}(\tilde{z})^2}} (\tilde{m}(\tilde{z}), 0, 1). \quad (8)$$

If $\tilde{m}(\tilde{z}) = 0$ i.e. $\lambda \tilde{z} = 1$ then the vector $\tilde{\mathbf{m}}$ is parallel to the free surface normal \mathbf{e}_z .

2.2. Linear analysis

The nonlinear advection equation model is linearized about the rotation axis $\tilde{\mathbf{x}}$ using the eigenvalue equation $[B - I\omega(\tilde{z})]\mathbf{k} = 0$ where $B = (\nabla v)^T$ and I is the identity tensor. One eigenvalue is zero, so the solution is constant and we set the associated eigenvector to be zero. The two other eigenvalues are always imaginary and lead to a solution to the linear equation of the form

$$\begin{aligned} \mathbf{x}(\theta(\tilde{z})) &= (x, y, z) \\ &= \left(\frac{\cos \alpha}{\omega(\tilde{z})} \sin \theta(\tilde{z}), \cos \theta(\tilde{z}), -\frac{\tilde{m}(\tilde{z}) \cos \alpha}{\omega(\tilde{z})} \sin \theta(\tilde{z}) \right), \end{aligned} \quad (9)$$

where $\theta(\tilde{z}) = \omega(\tilde{z})t$ is the phase angle with frequency

$$\omega(\tilde{z}) = \cos \alpha \sqrt{1 + \tilde{m}(\tilde{z})^2}. \quad (10)$$

Since the eigenvalues are determined by linearizing the nonlinear model and have no real parts we cannot determine the stability of the system.

Using Eqs. (6) and (7) we see that $\mathbf{x} \cdot \tilde{\mathbf{m}} = 0$ so that the fixed point axis is the liquid rotation axis. Then the trajectories, $\mathbf{x}(\theta(\tilde{z}))$, are a family of two-dimensional elliptic surfaces of constant radius, $|\mathbf{x}(\theta(\tilde{z}))| = 1$, similar to solid body rotation. The difference between this flow and solid body rotation is that the orientation of the streamlines and speed depend on their vertical location. We see from Eq. (10) that the critical point location where $\omega(\tilde{z}_{\text{crit}}) = 1$ is at $\tilde{z}_{\text{crit}} = 0$.

The horizontal distance between the intersection of the rotating fluid and solid body rotation point axis, $\tilde{\mathbf{x}}(\tilde{z}_{\text{crit}} = 0, \alpha)$, and the rotating fluid rotation axis, $\tilde{\mathbf{x}}(\tilde{z} = 1/\lambda_{\text{crit}}(\alpha) = 2 \sin \alpha)$, diverges as

$$\Delta \tilde{x} = \sin \alpha \tan \alpha. \quad (11)$$

So while the vertical height of the rotation axis is bounded, $0 < 1/\lambda_{\text{crit}}(\alpha) < 2$, with changing tilt angle, the horizontal dimension of the rotation axis diverges like $\tan \alpha$. Therefore, for large α but less than $\alpha = \pi/2$, we would expect a mix of considerable volume of fluid by periodic shearing.

The rate of mixing, based on our linear analysis, using Eqs. (9) and (11), with $\omega(1/\lambda) = \cos \alpha$, is

$$\frac{1}{\Delta t_{\text{max}}} \propto \frac{\dot{\Delta} \theta}{A(\Delta t_{\text{max}}(\alpha))} = \frac{1 - \cos \alpha}{2 \tan \alpha}. \quad (12)$$

The number of rotations to completely mix the domain is then Δt_{max} since we chose to scale the time by the rotation frequency. This quantitative estimate for the rate of mixing can be compared with trends seen in the experimental data presented and discussed in the following sections.

We note here that mixed cross-sectional area size increases exponentially, suggesting that the rate of mixing per unit area is zero for $\alpha = 0$ and also $\alpha = \pi/2$ because $\Delta\omega(\alpha = 0) = 0$ and $A(\alpha \rightarrow \pi/2, \Delta t_{\text{max}}) \rightarrow \infty$, respectively. Then if the rate of deformation per unit area is not always zero there must be a maximum for $\alpha \in (0, \pi/2)$. To determine the location of the maximum we take the derivative of $1/\Delta t_{\text{max}}$ with respect to

α and determine the zero of the resulting algebraic equation, $\cos \alpha (\sin^2 \alpha + 1)$. So the maximum should occur at an angle of about $\alpha = 52\pi/180$ from this analysis. This is the angle where the mixing would be the most efficient because it would require the least amount of time to mix $A(\alpha = 52\pi/180, \Delta t_{\text{max}})$. We will measure the rate of mixing using experimental Poincaré maps and test to see if this estimate is correct along with Eq. (12).

2.3. Results

While the solutions to Eq. (5) are not a good model for the full three-dimensional problem, they do provide us with some qualitative analysis of what to expect from this type of flow. Since the functions describing the rate $\dot{\mathbf{x}}$ are continuous functions we are guaranteed unique solution to Eq. (5) for a given set of initial conditions. Solutions to the nonlinear equation are found using an implicit fourth order Runge–Kutta algorithm with explicit starter (Sanz-Serna and Calvo, 1994). The equation is integrated to machine precision which is needed to ensure that the trajectories do not drift to other nearby trajectories and give false results of volume filling solutions. Fig. 2(a) and (b) shows plots of some of the streamline like contour curves that are the trajectory solution, $\mathbf{x} = \mathbf{x}(t)$, to Eq. (5) with initial conditions as listed in the caption. These are plotted in the vicinity of the liquid rotation axis and the tangent vector, $\tilde{\mathbf{m}}$, is also shown for clarity. In Fig. 2(a), we see that most of the trajectories do not lie in a single plane, so there are no streamlines for $|\mathbf{x}_0 \gg 0|$. This is true for the trajectories, *B*, *C*, and *D*, which also begin to lose eccentricity as the initial condition is extended away from the fixed point as shown in Fig. 2(b). The amount of deformation depends on the \tilde{z} location, but the type of deformation is similar all along the liquid rotation axis, except for $z = 1/\lambda$, because the free surface is flat so that the trajectories there are indeed streamlines.

A consequence of these nonlinear trajectories is that there may be some small flow in the direction tangent to the liquid rotation axis, $\tilde{\mathbf{m}}$. The weak velocity gradient may generate vortices, that transport fluid tangent to the liquid rotation axis only a short distance away. An estimate for the secondary flow, Fig. 2(c), is found by taking the scalar product of the liquid rotation axis tangent vector with the local velocity, $\tilde{\mathbf{m}} \cdot d\mathbf{x}/dt$, evaluated along a trajectory, $\mathbf{x} = \mathbf{x}(t)$, versus normalized angular location $\theta/2\pi$. The initial conditions are chosen so that they initially lie in a plane perpendicular to the liquid rotation axis, i.e. $\mathbf{x}_0 \cdot \tilde{\mathbf{m}} = 0$. The plot shows that the trajectory closest to the liquid rotation axis, *A*, has the smallest amplitude while the farthest point, *D*, has the largest. We also see that the maximum amplitudes are not symmetric on quarter domains, since the amplitude for $0 < \theta/2\pi < 0.25$ is larger than what happens on the opposite domain $0.5 < \theta/2\pi < 0.75$. This suggests that if vortices are generated then the gradient flow that will transport fluid along the rotation axis depends on the plane as we see in Fig. 2(c), since the direction is toward the free surface for $0.25 < \theta/2\pi < 0.5$ and $0.75 < \theta/2\pi < 1$, and toward the solid body rotation axis on the other opposite domains.

But, in the vicinity of the liquid rotation axis the flow is approximately two-dimensional and the trajectories are stream-

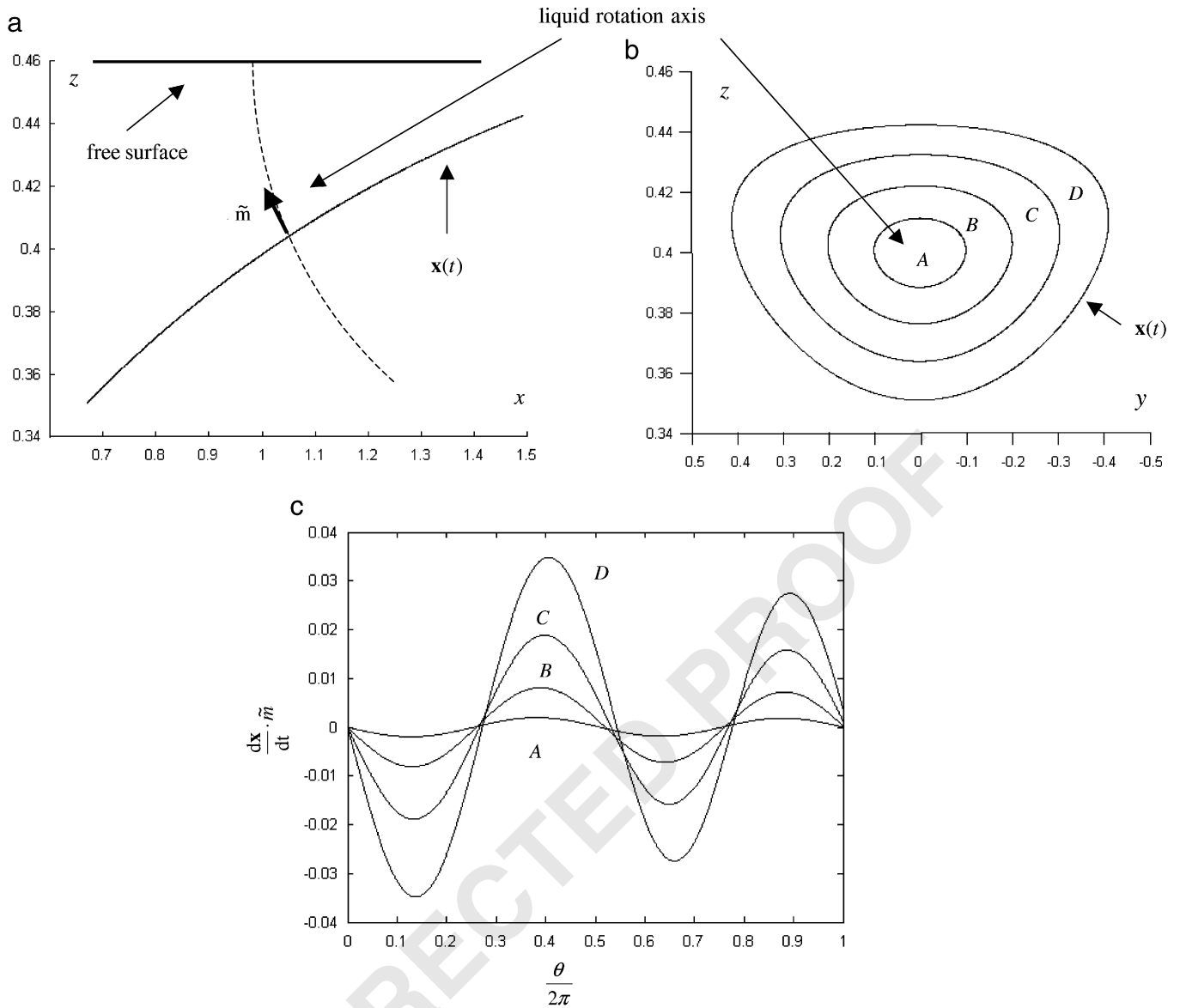


Fig. 2. Plots of solutions to Eq. (5) about the liquid fixed point axis for $\alpha = \pi/6$. (a) and (b) are two views of trajectories with initial conditions \mathbf{x}_0 : (A) (1,0.1,0.1), (B) (1,0.2,0.1) (C) (1,0.3,0.1), and (D) (1,0.4,0.1). The trajectories do not lie in a plane so the velocity along a trajectories is not perpendicular to the liquid rotation axis at large $|x| \gg 0.01$ distances. (c) Variations in velocity tangent to the liquid rotation axis, $dx/dt \cdot \tilde{\mathbf{m}}$, for the four initial conditions presented in (b).

1 lines according to our linear solution, Eq. (9). In this region
 2 there is periodic shearing, which is the proposed mechanism
 3 that generates mixing in the tilted rotating tank. Fig. 3 shows
 4 plots of a material line illustrating the periodic shearing process
 5 that occurs near the rotation axis as it deforms with increasing
 6 time. These plots are generated with the initial material line
 7 lying in the same plane as the rotation axis. The time interval
 8 is chosen to be near the natural frequency when the two ex-
 9 tremums sample the same plane, $\Delta\theta = 2\pi$. We see that as time
 10 advances, so does the displacement between nearby trajec-
 11 tories. The material line can never lie in the initial plane for time
 12 $t > 0$ because the rate of deformation, $\Delta\theta$, is positive for all
 13 $\alpha > 0$. The material line begins to fill a tubular surface, that is,

a plane wrapped around the rotation axis, as time approaches
 infinity in Fig. 3(f). This same process is true for the second
 order flow since those trajectories do not travel tangentially along
 trajectories with the same speed as the nearby ones.

3. Experiments

3.1. Setup and procedure

Experiments were performed using a cylindrical acrylic tank
 approximately 3 in in diameter and 48 in long. The tank was
 mounted on a large piece of acrylic using plastic dampers. A
 solid cylindrical piece was used as an end cap and to mount the

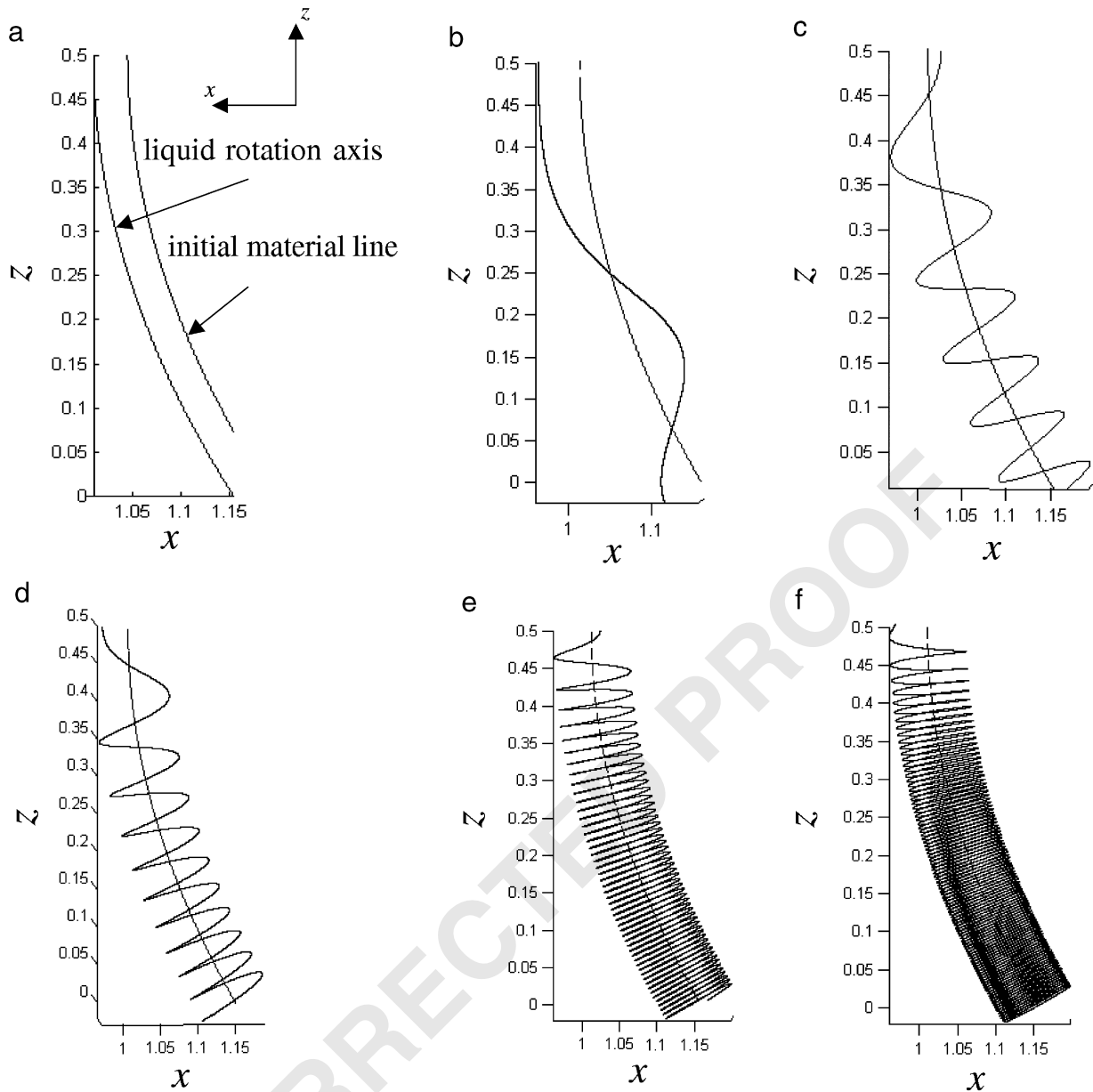


Fig. 3. Plot of analytical solutions to the trajectory equation, $\mathbf{x}(\theta)$, about the fixed point axis, $\bar{\mathbf{x}}(\bar{z})$, for $\alpha = \pi/6$. The extremum samples the same plane every $\Delta t = 47$. The plots are shown relative to this natural frequency at times $t =$ (a) 0×47 , (b) 1×47 , (c) 5×47 , (d) 10×47 , (e) 50×47 , and (f) 100×47 . There are 5×10^5 initial conditions in each plot.

1 cylinder on the motor. The end cap has a large hole drilled in this slot. The motor
 3 was mounted on a piece of acrylic with a hole for the drive shaft which attaches to the metal bar with a custom fabricated
 5 coupling. A schematic of the experimental setup is shown in Fig. 4. With such a long tube the coupling must be adjusted
 7 before each experiment to ensure that the shaft is parallel with respect to the tube. The motor is tested and set to rotate with
 9 a constant frequency of approximately 0.1 Hz. At the top of the acrylic mounting piece was a mounting plate with a small
 11 hole drilled for the laser. A planar laser sheet was generated using a lasiris laser (StockerYale) which emits a green sheet
 13 (wavelength 533.1 nm) at a constant output power of 5 mW.

The fluid is pure glycerol (Clearco) which has a viscosity of approximately 0.93 Pa s and a density of 1260 kg/m^3 at room
 15 temperature of 20°C , both numbers taken from tabulated values. A small portion of the glycerol was dyed with laser grade
 17 Rhodamine B (Sigma-Aldrich) until the solution becomes a uniform clear, but fluorescent, color. The dye solution must
 19 be kept from ambient light which causes the dye to degrade and the luminescence to weaken in intensity. Based on our
 21 physical parameter, dimensions, and motor speed we estimate the Reynolds number to be approximately 0.1 for our experi-
 23 ments, and $0.3 < \lambda < 0.75$. The capillary number is approximately $Ca = 0.07$ with an air–glycerol–acrylic surface tension
 25 of approximately 55 mN/m taken from tabulated values.

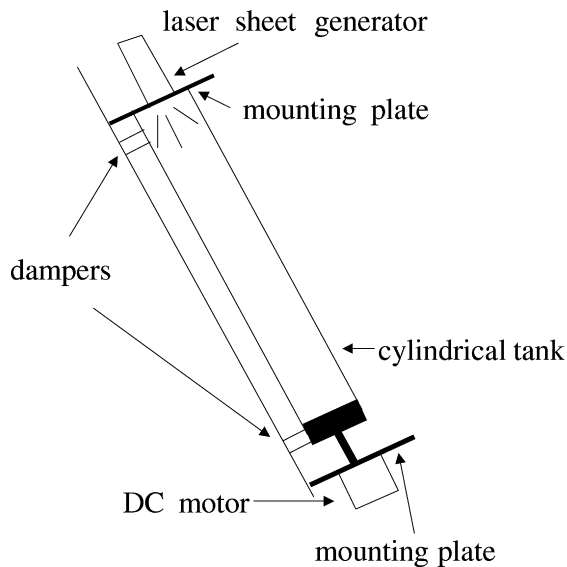


Fig. 4. Experimental setup.

The experimental Poincaré maps were generated by, first, filling the tank with a known volume of fluid. Then the distance from the free surface to the minimum fluid location in the tank was measured and recorded. A small blob of the dye solution was placed near the free surface and the laser was placed in the mounting plate. The laser sheet was placed so that it illuminated the $y = 0$ plane which is where, according to our theory, the liquid rotation axis lies. The motor was turned on and the flow plane perpendicular to the laser sheet was viewed from the side using a CCD camera (Sony X710). There was some optical distortion since the glycerol and acrylic are not index matched, but the indices of refraction are similar and the optical distortion was minimal. Images were taken in set intervals of 10 s for approximately 10^4 s, so each experimental run contains nearly 10^3 frames. This is an important tool for measurement since we can determine the precise number of rotations that produce a certain amount of mixing in our tank. The steady-state values, Δt_{\max} , are typically reached before the end of each run. To ensure that we do reach a steady state the mixed area is estimated as a function of time for several experimental Poincaré maps and plotted as a function of time. Plots of these results are shown in Figs. 5 and 6.

3.2. Experimental results and discussion

Fig. 5 shows experimental Poincaré sections of the mixed domain. In all of the images shown, the fluid appears very well mixed over the domain spanning the free surface. Also, the liquid rotation axis appears in all of the images suggesting that our nonlinear expansion was valid. The fluorescent blob is also well mixed in the vortex region near the walls that appears to be KAM like surface generated by the nonlinear flow near the rotation axis. It is not clear if these surfaces are truly KAM because they appear to mix in a finite time. Typically the only way to move fluid from KAM regions into the bulk is only

by diffusion (Fountain et al., 2000; Alvarez-Hernández et al., 2002). While the initial blob was always placed along the free surface we do not observe the separation of the two regions for $\lambda < \lambda_{\text{crit}}$ so that the KAM surfaces are possibly being broken up by periodic shearing. Also, while the vortices are generated by interaction of the curved streamlines with the wall, they do not appear to be Moffatt (1964) vortices. The similarities in structure of the vortices is also an indication that they are not Moffatt types since they do not vary with a change in the liquid level and therefore do not produce a cascade of vortices but rather a single large vortex on either side of the liquid rotation axis.

The first sequence of images, Fig. 5(a)–(d), shows the steady-state images, i.e. $\Delta t_{\max}(\alpha)$, for $\alpha = 15\pi/180$ at $\lambda = 0.30, 0.38, 0.50$, and 0.75 , respectively. The first images, Fig. 5(a) and (b), look nearly identical despite the fact that they were run at different liquid heights. But the final images for Fig. 5(c) and (d) look slightly different at their maximum time elapsed. This visual difference is possibly due to wall effects which begin to slightly affect the results as $\lambda \rightarrow \lambda_{\text{crit}}$.

The next group of images, Fig. 5(e)–(h), are steady-state mixing images for fixed liquid level of $\lambda = 0.30$ and tilt angles of $\alpha = 25\pi/180, 45\pi/180, 55\pi/180$, and $65\pi/180$, respectively. For all of these images it appears that $\lambda < \lambda_{\text{crit}}$, as expected. At small tilt angle, Fig. 5(e), the mixed domain size is small when compared to the larger angles. Also, for the smallest tilt angle, Fig. 5(e), the KAM surfaces generated by the vortices are relatively small. The mixed domain size increases with increasing α for all angles shown in this sequence. The size of the KAM like regions also increases with increase in tilt angle, but the size of the mixed area increase is larger. This is clearly seen in Fig. 5(g) and (h), where the KAM region is confined to a small and also well-mixed region. Typically, these KAM surfaces may be the last or first regions to become mixed depending on the initial conditions. But they do mix in a finite time, which is an important feature of this periodic shearing flow. The inset in Fig. 5(h) also reveals some of the characteristics of periodic shearing that were illustrated in Fig. 2. The inset is a close-up view of flow near the liquid rotation axis. The image clearly shows the helical-type flow that is predicted near the rotation axis. Actually all of the flows show these characteristics, but the helical-type flow is difficult to visualize from static images.

The last group of images, Fig. 5(i)–(l), are steady-state images for $\lambda = 0.75$ and 0.50 at tilt angles as listed in the caption. For this set of data it appears that $\lambda \geq \lambda_{\text{crit}}$ since all of the domains are completely mixed. The images do show the same liquid axis of rotation and KAM surfaces as in the previous examples. Since we cannot determine if we are at, or greater than, the critical tank height we will not include these examples in the comparisons with theory. Instead they are presented to show that the domain typically mixes completely despite any wall effects.

Fig. 6 shows plots of the mixed area versus elapsed time at various tilt angles and dimensionless liquid levels, for all λ . The values are generated using the experimental Poincaré maps. An algorithm utilizing threshold limits was written using MATLAB. The threshold was set by first performing the algo-

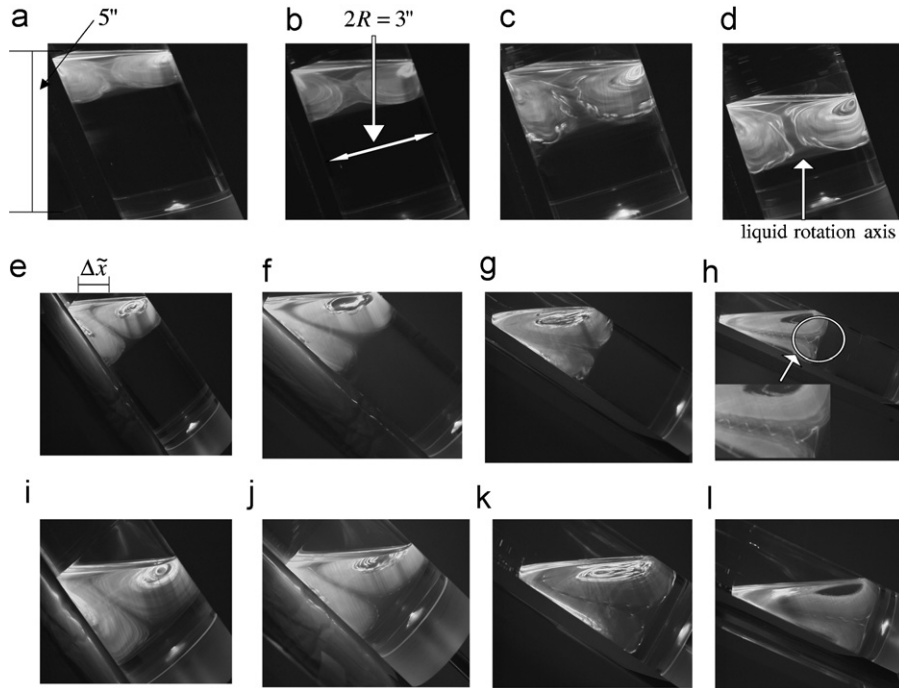


Fig. 5. Experimental Poincaré sections of an initial blob of dye as it intersects the xz -plane at $y=0$. The first row were all taken at fixed time $\Delta t \approx 1000$ and angle $\alpha = 15\pi/180$ with $\lambda =$ (a) 0.30, (b) 0.38, (c) 0.50, and (d) 0.75. The second row are images for fixed time $\Delta t \approx 1000$ and $\lambda = 0.30$ at angles $\alpha =$ (e) $35\pi/180$, (f) $45\pi/180$, (g) $55\pi/180$, and (h) $65\pi/180$. The last row are images for fixed time $t \approx 1000$ and $\lambda = 0.75$ at angles $\alpha =$ (i) $35\pi/180$, (j) $45\pi/180$, and $\lambda = 0.50$ at angles (k) $55\pi/180$ and (l) $65\pi/180$.

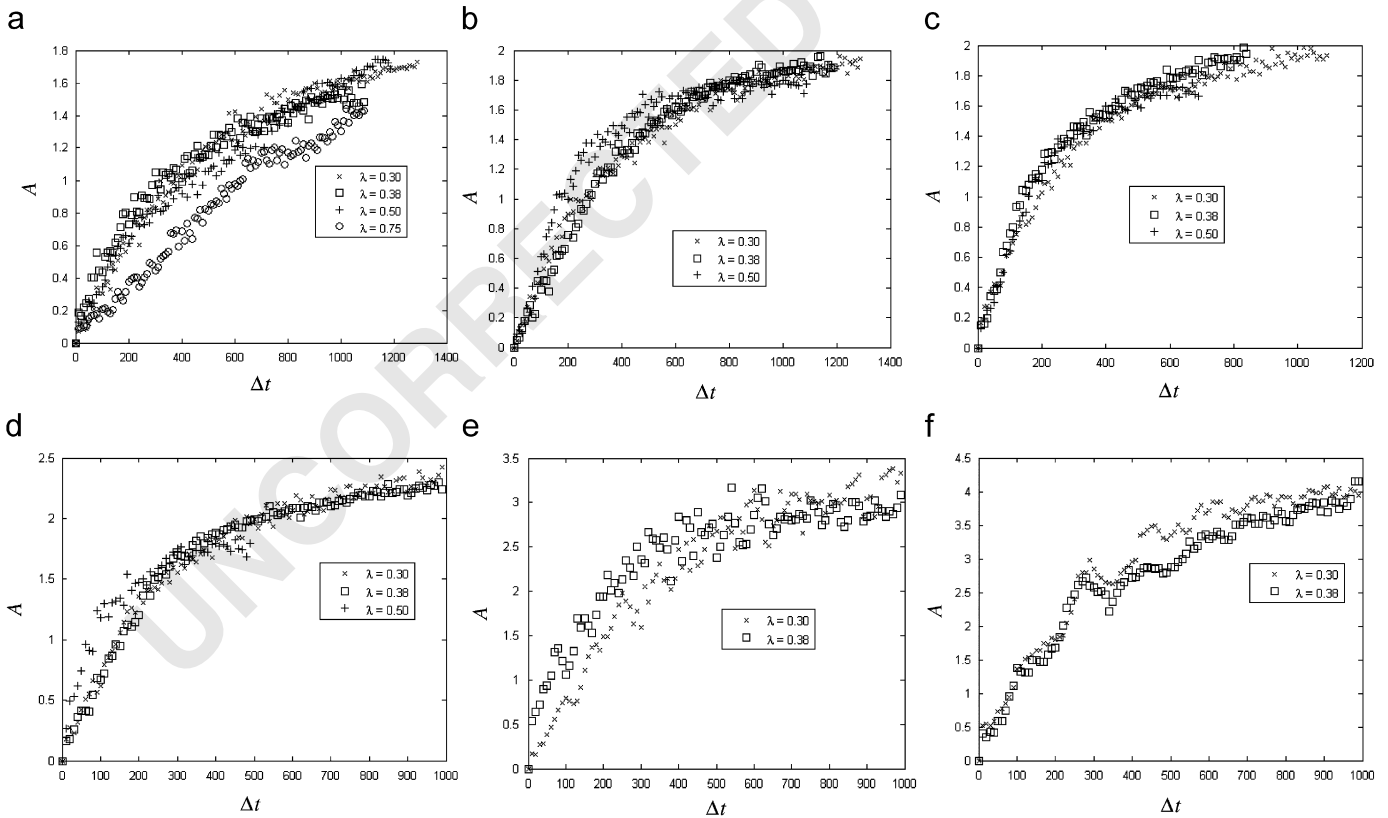


Fig. 6. Plot of the mixed area versus time for $\lambda = 0.30$ (\times), 0.38 (\square), 0.50 ($+$), and 0.75 (\circ) with tilt angles $\alpha =$ (a) $15\pi/180$, (b) $25\pi/180$, (c) $35\pi/180$, (d) $45\pi/180$, (e) $55\pi/180$, and (f) $65\pi/180$. The largest λ values in (a) correspond to a value near the measured critical value. Note that the y -axis has a different scale in each of the panels.

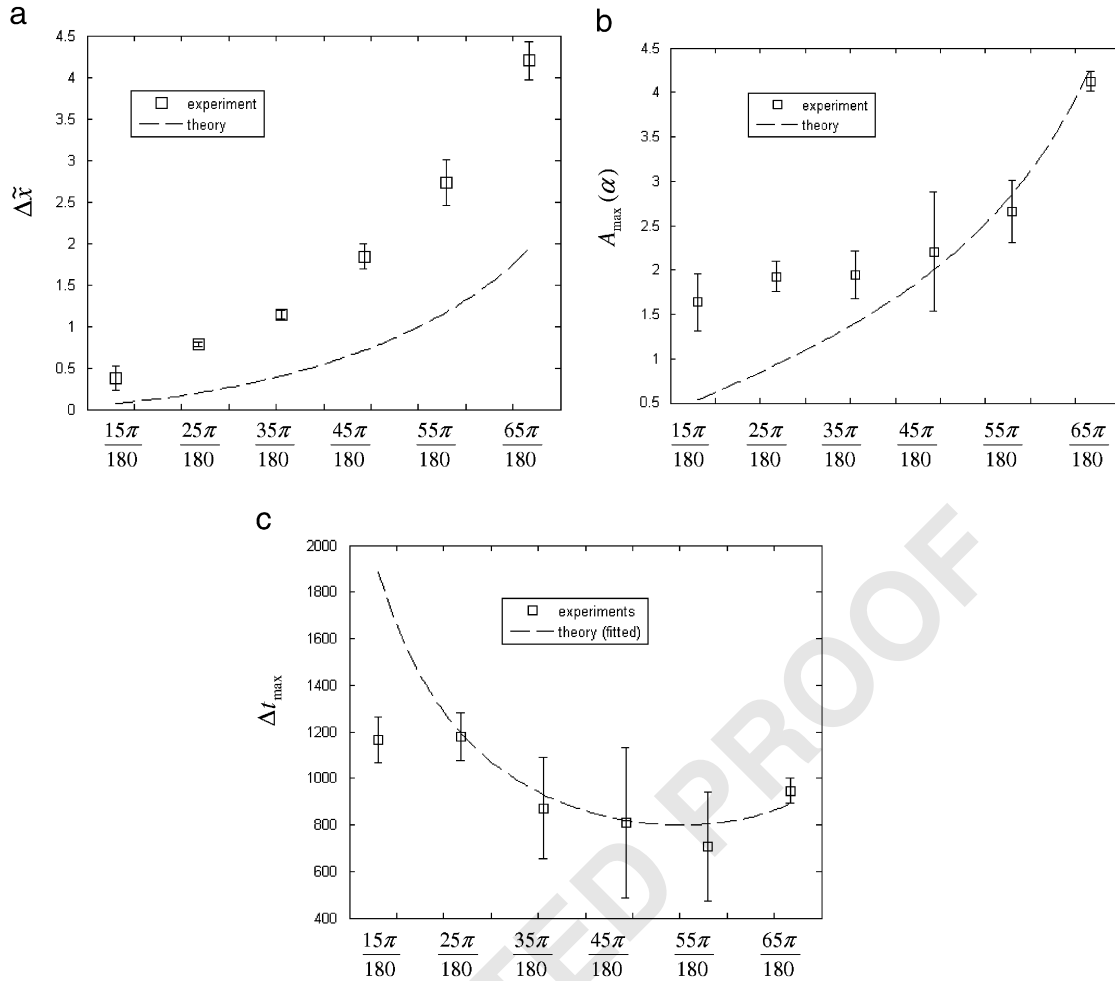


Fig. 7. (a) Experimentally measured horizontal dimension of fixed point axis versus α . The solid line is the theoretical prediction. (b) Dimensionless mixed area, measured from Poincaré maps, versus α . The solid line is the theoretical prediction. (c) Dimensionless mixing time $\Delta t_{\max} = C_0(1 - \cos \alpha)/2 \tan \alpha$ versus α . The constant, $C_0 = 120$, is the best fit value.

1 rithm on an image at a given time elapsed. Once this threshold
 2 value was found then all of the images for a given experiment
 3 were analyzed with the same threshold value with little differ-
 4 ence between experiments. The first plot, Fig. 6(a), shows time
 5 elapsed data for $\alpha = 25\pi/180$ at four different values of λ . The
 6 data collapse for the smallest values of λ in this first plot. The
 7 data, in Fig. 6(a), also collapse for the largest value, $\lambda = 0.75$,
 8 but the wall effects (see Fig. 5(d)) seem to only slightly modify
 9 the slope of the curve to something that has more of a linear
 10 shape than the other data curves on the same graph. Overall,
 11 the data tend to collapse in each of the plots, Fig. 6(b)–(f), re-
 12 gardless of the value of λ which is the same as in Fig. 6(a).

13 3.3. Comparison with theory

14 All of the data presented in Fig. 7 are averaged over λ for
 15 a given α , for qualitative comparison with our proposed fixed
 16 point axis and periodic shear driving force theory. The first plot,
 17 Fig. 7(a), shows the horizontal distance of the fixed point axis,
 18 $\Delta\bar{x}$, measured over the mixed domain, versus α . The error bars
 19 are the standard deviation measured over λ . In this plot we see

20 that the theory underestimates the horizontal dimensions of the
 21 fixed point axis consistently by a factor of 2. But the shapes
 22 of the curves are similar and the theory and experiments show
 23 agreement that the distance diverges as $\alpha \rightarrow \pi/2$. Part of the
 24 error in this measurement is due to the optical distortion of the
 25 images taken in the glycerol filled tank, especially as the rota-
 26 tion axis moves away from the center plane. This information,
 27 along with the fact that this axis survives throughout the mix-
 28 ing process, suggests that the fixed point axis is the rotation
 29 axis as we have predicted.

30 The next plot, Fig. 7(b), is the dimensionless mixed area
 31 $A(\alpha, \Delta t_{\max})$, measured from the experimental Poincaré maps,
 32 versus α . The theory underestimates the mixed area at small α ,
 33 and is better for values near $45\pi/180$, and as $\alpha \rightarrow \pi/2$. Since
 34 the mixed area is calculated using threshold values it is difficult
 35 to determine what is a well-mixed region but the calculations
 36 do show the trend of an increase in the mixed area with angle at
 37 the threshold values used. The discrepancy is also due, in large
 38 part, to the secondary vortical flow which increases the mixed
 39 domain especially at smaller angles, but also tends to generate
 40 small KAM like surfaces that do not mix. So the largest angle

measured, $\alpha = 65\pi/180$, is closer to theory, in part because the KAM regions are smaller than the predicted mixed area, but the smallest angle measured $15\pi/180$ is underestimated possibly due to KAM surfaces as well.

The next plot, Fig. 7(c), shows the inverse of the dimensionless absolute time elapsed Δt_{\max} for the experimental Poincaré maps to reach a steady state. The minimum elapsed time is approximately 1×10^{-3} at an angle of $\alpha = 15\pi/180$. The maximum of 2.25×10^{-3} occurs at an angle of $\alpha = 55\pi/180$. But this data value has quite a bit of error associated with it and it is not conclusive that this is indeed the best value for mixing. Nevertheless, the two nearest data points, i.e. $\alpha = 45\pi/180$ and $65\pi/180$, seem to fit the curve just as well. The dimensionless time elapsed can be used to determine the exact number of turns, n_{\max} , needed to completely mix most of the domain spanning $1/\lambda_{\text{crit}}$ which is $n_{\max} = \Delta t_{\max}$ using our choice of non-dimensionalization with the rotation speed. So it takes nearly 2.5 times more turns to completely mix a smaller domain at $\alpha = 15\pi/180$ versus a larger area in the $\alpha = 45\pi/180$ case.

4. Conclusion

In this paper we focus our attention on the problem of fluid mixing in a partially filled-tilted rotating tank in the limit of small Reynolds and capillary number. The tilted rotating tank is analogous to a cement mixer, which requires only a single moving part and no impeller, so that it is ideal for mixing very viscous fluids and slurries. A detailed analysis of the flow field is not presented in this paper. Instead, an approximate nonlinear solution for three-dimensional solid body rotation in a tilted and partially filled tank is found, then linearized about a liquid rotation axis. This analysis suggests a similarity solution for the size of the three-dimensional domain, that is compared with experiments that exhibit large-scale fluid mixing. A knowledge of the mixed domain size is very useful for determining proper tank dimensions, and angle, with which one would expect to see fluid mixing. To date, there does not exist a single *a priori* analytical solution for the size of a mixed domain in a chaotic flow inside of a tank, and we have tried to present one for comparison with experiments.

Laser fluorescence experiments are performed using glycerol and Rhodamine B in a cylindrical acrylic tank nearly 3 in in diameter. The experiments are conducted by placing a small blob of dye near the top of the free surface and a single plane is illuminated via experimental Poincaré mapping. The experiments reveal the existence of the fixed point axis. The dimensions of the axis are compared with the theory at different tilt angles with very good qualitative agreement despite the appearance of KAM like surfaces that are generated by vortices. While the linear analysis does not predict these vortices the nonlinear model used to derive it does suggest that a secondary flow is generated by the flow in the vicinity of the fixed point axis.

The critical angle analysis may also be useful for those in industry that use cement mixers, since it is a number for the minimum number of rotations needed to completely mix a given cross-sectional area. So the slowly rotating tank may provide an energy efficient way to generating chaotic advection in tanks

used in large batch reactors. It will be useful to test the idea of mixing in tank by periodic shearing at higher Reynolds number, which may decrease the number of rotations needed to mix an area and, hence, speed up mixing time. The drawback though may come in the form of larger KAM surfaces that do not mix at all. Also, it would be beneficial to use particle tracking techniques to determine full velocity information which may reveal more interesting features of the slowly rotating flow.

Notation

A_{\max}	maximum mixed cross-sectional area	
B	velocity gradient transpose, $(\nabla v)^T$	
Ca	capillary number	
$\mathbf{e}_x, \mathbf{e}_y, \mathbf{e}_z$	Cartesian coordinate basis vectors	
\mathbf{e}_{zz}	vector perpendicular to tank rotation axis (parallel to tank vorticity)	
H_0	liquid height	
I	identity tensor	
$\tilde{m}(\tilde{z})$	tangent line to liquid rotation (fixed point) axis	
n_{\max}	total number of rotations needed to mix A_{\max}	
P	fluid pressure	
R	tank radius	
Re	Reynolds number	
t	parameter used to denote time	
\mathbf{v}	velocity vector	
$\tilde{x}(\tilde{z})$	horizontal location along liquid rotation axis	
x, y, z	denotes position in Cartesian coordinates	
$\tilde{z}, \tilde{z}_{\text{crit}}$	vertical location along liquid rotation axis	
<i>Greek letters</i>		
α	tilt angle where a zero value corresponds to a horizontal tank	
γ	surface tension at air–liquid–solid interface	
Δt_{\max}	time required to mix maximum area	
$\theta(\tilde{z})$	angular location of a circular trajectory rotation around liquid rotation axis by periodic shear	
$\lambda, \lambda_{\text{crit}}$	inverse dimensionless liquid height, R/H_0	
μ	fluid viscosity	
ρ	fluid density	
σ_i	stress tensor, $-P\mathbf{I} + \boldsymbol{\tau}$	
$\boldsymbol{\tau}$	Newtonian fluid stress tensor, $\mu(\nabla\mathbf{v} + \nabla\mathbf{v}^T)$	
$\omega(\tilde{z})$	rotation (periodic shear) frequency along liquid rotation axis	
Ω	tank rotation rate (Hz)	65

5. Uncited references

Fountain et al. (1998); Lamberto et al. (1996) 67

Acknowledgments

T.W. would like to acknowledge support for this work which was provided by the NSF VIGRE program. A.M. was supported on a grant from the UCLA NSF sponsored REU program (DMS-0601395).

1 **References**

- Alvarez-Hernández, M.M., Shinbrot, T., Zalc, J., Muzzio, F.J., 2002. Practical
 3Q5 chaotic mixing. *Chemical Engineering Science* 57, 3749–3753.
- Aref, H., 1984. Stirring by chaotic advection. *Journal of Fluid Mechanics*
 5 143, 1–21.
- Arnold, V.I., 1978. *Mathematical Methods of Classical Mechanics*. Springer,
 7 Berlin.
- Aubin, J., Xuereb, C., 2006. Design of multiple impeller stirred tanks for the
 9 mixing of highly viscous fluids using CFD. *Chemical Engineering Science*
 61, 2913–2920.
- Campolo, M., Sbrizzai, F., Soldati, A., 2003. Time-dependent flow
 11 structures and Lagrangian mixing in Rushton-impeller baffled-tank
 13 reactor. *Chemical Engineering Science* 58, 1615–1629.
- D'Alessandro, D., Dahleh, M., Mezic, I., 1999. Control of mixing in fluid
 15 flow: a maximum entropy approach. *IEEE Transactions on Automation
 and Control* 44 (10), 1852–1863.
- Fountain, G.O., Khakhar, D.V., Ottino, J.M., 1998. Visualization of three-
 17 Q4 dimensional chaos. *Science* 281, 683–686.
- Fountain, G.O., Khakhar, D.V., Mezic, I., Ottino, J.M., 2000. Chaotic mixing
 19 in a bounded three-dimensional flow. *Journal of Fluid Mechanics* 417,
 21 265–301.
- Franjione, J.G., Ottino, J.M., 1992. Symmetry concepts for the geometric
 23 analysis of mixing flows. *Philosophical Transactions of the Royal Society
 of London*, 301–323.
- Lamberto, D.J., Muzzio, F.J., Swanson, P.D., 1996. Using time-dependent
 25 RPM to enhance mixing stirred vessels. *Chemical Engineering Science* 51
 27 (5), 733–741.
- Moffatt, H.K., 1964. Viscous and resistive eddies near a sharp corner. *Journal
 of Fluid Mechanics* 18, 1–18.
- Sanz-Serna, J.M., Calvo, M.P., 1994. *Numerical Hamiltonian Problems*.
 31 London.
- Unger, D.R., Muzzio, F.J., Aunins, J.G., Singhvi, R., 2000. Computational
 33 and experimental investigation of flow and fluid mixing in the roller bottle
 bioreactor. *Biotechnology and Bioengineering* 70 (2), 117–130.

UNCORRECTED PROOF